Available online at www.sciencedirect.com
SCIENCE DIRECT®
International Journal of Heat and Mass Transfer 49 (2006) 2491–2501
International Journal of HEAT and MASS TRANSFER
www.elsevier.com/locate/ijhmt

Local heat transfer measurements of steam/air mixtures in horizontal condenser tubes

Tiejun Wu, Karen Vierow *

School of Nuclear Engineering, Purdue University, 400 Central Drive, West Lafayette, IN 47907 2017, United States

Received 18 March 2005; received in revised form 4 January 2006
Available online 22 March 2006

Abstract

Condensation of vapor/noncondensable gas mixtures in horizontal tubes is not well understood because condensate stratification and the multidimensional nature add to the complexity of the phenomena. The heat transfer and fluid flow phenomena in a horizontal condenser tube were experimentally studied, along with the heat transfer reduction effect of a noncondensable gas. The temperature gradient across the condenser tube wall was measured locally to investigate the asymmetrical heat transfer characteristics around the condenser tube periphery. The condensation heat transfer coefficients on the tube top were much greater than the values at the bottom and the noncondensable gas significantly reduced the heat transfer rate.

Keywords: Condensation; Noncondensable gas; Flow regime

1. Introduction

As one of the most widely used types of heat exchangers, horizontal condensation heat exchangers have traditionally found many industrial applications, including in the process industry, the air conditioning and refrigeration industry, and for condensation of mixed vapors for distillation of hydrocarbons [1].

In the nuclear industry, horizontal heat exchangers are also widely used. Recently, a horizontal heat exchanger design has been proposed for a passive containment cooling system (PCCS) of future light water reactors [2]. Current PCCS designs typically employ a vertical condenser [3,4]. The horizontal design is proposed because horizontal heat exchangers have a potentially higher heat removal capability than vertical heat exchangers [5].

The details of condensation heat transfer in the presence of a noncondensable (NC) gas in horizontal condenser tubes are not well understood. Compared to the well-studied case of in-tube condensation for vertical downflow [6,7], the complication of this phenomenon mainly comes from two factors. The first is the nonsymmetrical two-phase phase distribution in the tube cross-section. Also, within the gas phase, when the velocity is low, the asymmetrical noncondensable gas concentration caused by the density difference between the noncondensable gas and steam could affect the heat transfer [8]. For flow regimes with low gas-phase superficial velocity, the heat transfer characteristics at the top and bottom of the tube are quite different, and thus the heat transfer coefficients are also different. The second factor is the mode of condensate drainage. In a horizontal tube, condensate must be carried out by its own momentum or by shear from the steam/gas mixture whereas gravity draining occurs in a vertical tube.

Many researchers have investigated in-tube condensation for horizontal heat exchangers [2,9–12]. Nakamura [2] performed experiments on steam/air mixture condensation in a horizontal U-tube under typical PCCS operating conditions and measured the cross-section-averaged heat transfer coefficients. Chato [9] performed experiments on

* Corresponding author. Tel.: +1 765 494 4576; fax: +1 765 494 9570.
E-mail address: vierow@ecn.purdue.edu (K. Vierow).

0017-9310/$ - see front matter © 2006 Elsevier Ltd. All rights reserved.
doi:10.1016/j.ijheatmasstransfer.2006.01.025

Nomenclature

F	criteria for flow regime identification
g	gravitational acceleration (m/s^2)
h	heat transfer coefficient (W/m^2/K)
k	thermal conductivity (W/m/K)
N	number of tubes
q''	heat flux (W/m^2)
Q	heat transfer rate (W)
r	radius (m)
T	temperature (°C)
z	axial location (m)

Greek symbols

δ	film thickness (m)
ρ	density (kg/m^3)
τ	shear stress (N/m^2)

Subscripts

bot	bottom of the tube
cl	centerline
co	coolant
l	liquid
top	top of the tube
w	wall
wall,in	physical inner surface
wall,out	physical outer surface
wi	inner surface thermocouple
wo	outer surface thermocouple
*	location on the tube, can be "top" or "bot"

pure steam, laminar flow condensation in a horizontal tube and developed a mechanistical model for the overall heat transfer coefficient. Shah [10] developed an empirical correlation for the heat transfer coefficient for annular flow condensation of pure steam. Dobson and Chato [11] developed a flow regime map and heat transfer models for condensation of pure refrigerants in a small diameter tube. Ueno et al. [12] described their thermal hydraulics tests of condensation in a horizontal tube under LOCA conditions in a PWR and developed empirical correlations for the heat transfer coefficient. However, other than the work by Nakamura [2] which obtained tube section-averaged data, there were no experimental investigations that fully covered the PCCS conditions of interest with the presence of a noncondensable gas. More significantly, there are no reported measurements of a truly local heat transfer coefficient in horizontal tubes except for the limited data by Rosson and Meyers [13] for refrigerants.

The effect of a NC gas on condensation heat transfer has been extensively studied both experimentally and theoretically for simple geometries as on a vertical flat plate and in vertical tubes. Degradation factor correlations have been developed from experimental data to account for the effect of a NC gas in vertical tubes [6,14]. A semi-empirical diffusion layer model has been developed by Peterson et al. [15] for condensation inside vertical tubes. However these correlations and models are highly dependent on specific experimental conditions and the vertical orientation.

The research herein was initially conducted to support the horizontal PCCS design and was extended for general application to other horizontal heat exchangers. In the experiments, the local heat transfer coefficient profiles along the condenser tube were measured to provide a comprehensive database for the phenomena and to support the development of analysis models.

2. Experimental facility

2.1. Test loop and system instrumentation

As shown in Fig. 1, the major components of the test facility are: the steam generator, the NC gas supply line, the coolant water supply, the test section, the condensate collection system, the associated piping and water storage tanks, the instrumentation and the data acquisition system. All heated components except the test section secondary side are thermally insulated with fiberglass insulation.

Steam exits the steam generator and passes through a separator that removes water droplets. Prior to mixing with the NC gas, the steam flow rate is measured with a vortex flow meter. Air is used as the NC gas. Two mass controllers of different ranges control the air flow rate. A heater installed downstream of the mass flow controllers preheats the air to the prescribed temperature. The steam/air mixture then enters the condenser tube and steam is condensed by the coolant water flowing in the coolant annulus. At the condenser tube exit, condensate is collected in the condensate collection tank. The condensate flow rate is calculated from the rate of water level rise in a sight glass on the tank. At the test section exit, steam and NC gas are vented through a control valve which is manually adjusted to maintain the test section inlet at a constant pressure.

Filtered city water is used for the secondary-side cooling water supply. To ensure a uniform flow of coolant through the coolant annulus, coolant enters and exits through four ports, located 90° apart. A magnetic flow meter measures the coolant flow rate.

The test section is a double pipe, countercurrent flow, concentric-tube heat exchanger. The inner tube is the condenser tube and the secondary-side coolant water flows through the surrounding coolant annulus countercurrent to the primary fluid. The condenser tube is a 4.5 m long

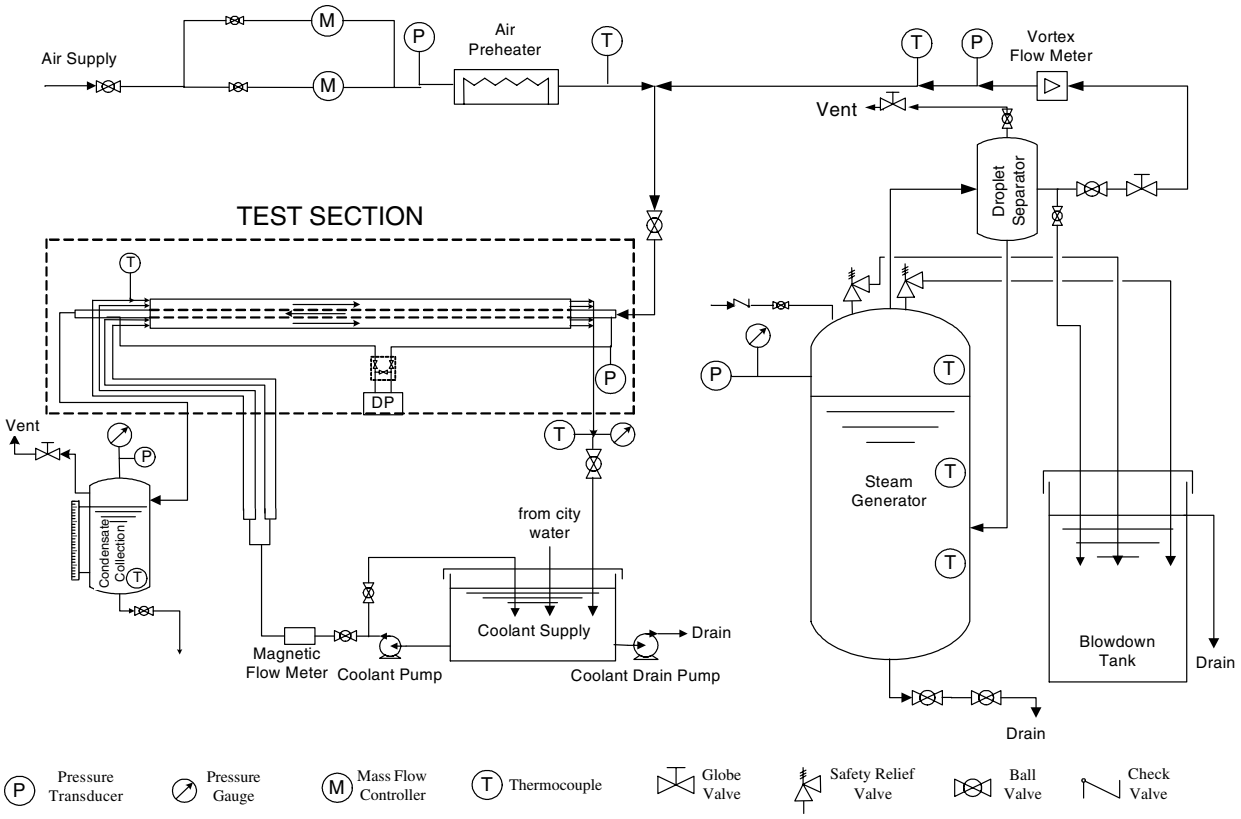

Fig. 1. Test facility layout.

SS304 tube of 31.7 mm OD and 2.1 mm wall thickness with a heat transfer length of 3.0 m. The coolant annulus outer diameter is 63.5 mm.

2.2. Test section instrumentation

The centerline, tube and coolant thermocouples were placed at 14 axial locations along the test section. These locations are closely spaced near the condenser tube inlet and spaced further apart with distance from the inlet, with the axial locations shown later in Fig. 7. Thermocouples were placed along the upper and lower sides of the test section. The thermocouple locations at each of the 14 cross-sections are shown in Fig. 2, where z is defined as the length from the start of the heat transfer region.

Condenser tube centerline temperatures are measured with 1.0 mm T-type (copper–constantan) sheathed thermocouples. For the condenser tube outer surface temperatures, a 0.5 mm groove was made on the condenser tube outer surface and a 0.5 mm sheathed thermocouple was silver soldered into the groove. Coolant temperatures are measured with 1.0 mm sheathed thermocouples. The sheathed thermocouples have an accuracy of ±0.5 °C per manufacture specifications.

For condenser tube inner surface temperatures, a hole was drilled nearly through the tube wall and a thermocouple with a plug design was tapped into the hole. Caution was taken in drilling the hole not to deform the tube inner surface. The plug is made of the same material as the condenser tube. To have good thermal contact between the plug and the tube, the hole was filled with high thermal conductivity silver epoxy ($k \approx 29.0$ W/m/K) before tapping the plug in. T-type thermocouple wires of 0.25 mm diameter were threaded through holes in the plug and soldered together to form the measurement junction. The details of the plug thermocouples are provided in Fig. 3. These

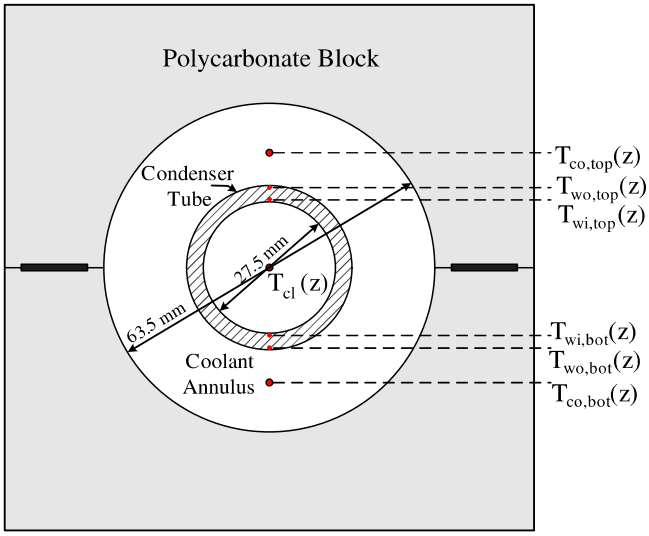

Fig. 2. Temperature measurement cross-section.

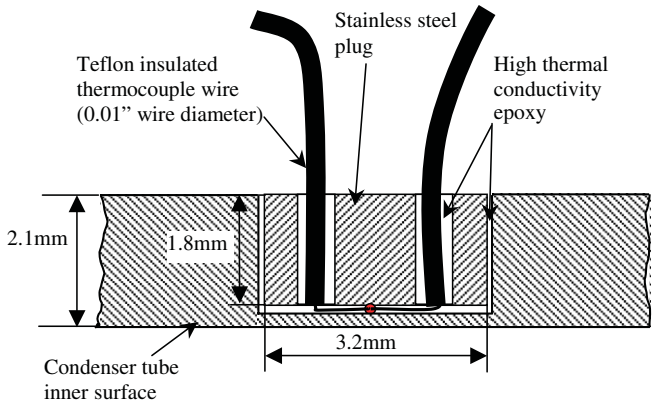

Fig. 3. Details of the tube wall inner surface temperature thermocouples.

in-house designed plug thermocouples were calibrated and the differences between the readings from the thermocouples were within ±0.2 K under isothermal conditions.

3. Calibration of thermocouple pairs for heat flux measurement

The local wall heat fluxes on the condenser tube are measured by the wall inner surface-to-outer surface thermocouple pairs. Ideally a heat conduction calculation as in Eq. (1) should give the local wall heat flux:

$$q''_{\text{wall,in},*}(z) = \frac{k_{\text{w}}(T_{\text{wi},*}(z) - T_{\text{wo},*}(z))}{r_{\text{wall,in}} \ln\left(\frac{r_{\text{wo}}}{r_{\text{wi}}}\right)} \quad (1)$$

The subscript "*" can be "top" or "bot", $q''_{\text{wall,in}}$ is the local heat flux based on the inner diameter of the tube and r is the radial position. The calculated local heat fluxes from preliminary test results had large fluctuations in axial profiles, which indicated large uncertainties. The error arose from trying to measure a heat flux via the temperature gradient across a tube wall which has a thickness of only about 2.1 mm. The error in the location of the surface temperature thermocouples r_{wi} and r_{wo} are important for a small wall thickness. Thus the thermocouple pairs used to measure the local heat fluxes needed to be calibrated individually.

The calibration device and setup as shown in Fig. 4 was used to perform the heat flux calibration. The main parts of the calibration setup are the boiling section and the condenser. The condenser tube was set vertically to eliminate asymmetrical effects. The boiling section is made of a 0.254 m long, 4 in. Schedule 10 stainless pipe with flanges attached on both ends. By moving the boiling section along the condenser tube, the thermocouple pairs can be calibrated, two pairs at a time. The coiled tube condenser has a capacity that is high enough to condense all of the steam generated from the boiling section.

Before each calibration test, the boiling section was filled with water up to a level close to the top of the boiling section. During the run, while steam of a given pressure and

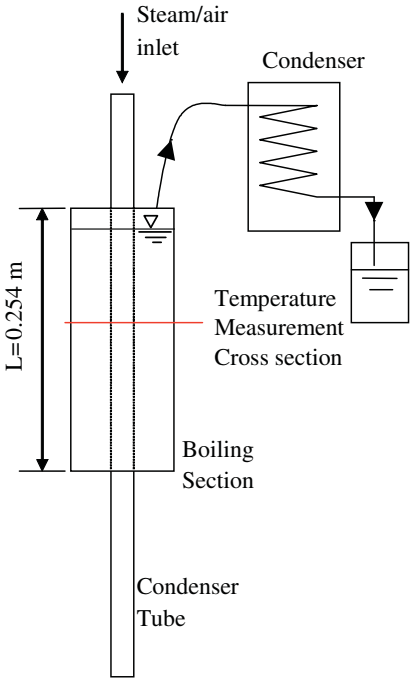

Fig. 4. Calibration device and setup.

flow rate traveled through the condenser tube, the water in the annulus was heated to the saturation temperature. The water that was boiled off in the boiling section was condensed by the condenser and then collected in a graduated cylinder. The time-averaged boiling rate was calculated by simply dividing the collected water mass by the collection time. From the boiling rate, time-averaged heat transfer rate was calculated. The heat loss from the calibration section was estimated to be about 20.0 W [16]. The heat loss is accounted for by adding this amount to the calculated heat transfer rate obtained from the condensation collection rate. The heat flux was determined by dividing the total heat transfer rate by the heat transfer area. By changing the primary steam pressure and flow rate, different heat fluxes could be obtained.

The time-averaged inner surface-to-outer surface temperature differences were compared with the heat fluxes. A linear fit between the heat flux and the temperature difference provided the calibration curves for the inner surface-to-outer surface thermocouple pairs. The heat flux during the condensation experiments could then be calculated from these equations.

The calibration results for a typical temperature measurement cross-section are shown in Fig. 5. The figure shows that the wall heat flux is approximately a linear function of the temperature difference across the tube wall. Eq. (1) also shows that the wall heat flux is a linear function of the temperature difference across the wall if the thermal conductivity of the wall material is considered to be constant.

The error associated with the calculated heat flux and heat transfer coefficients is mainly caused by the uncertain-

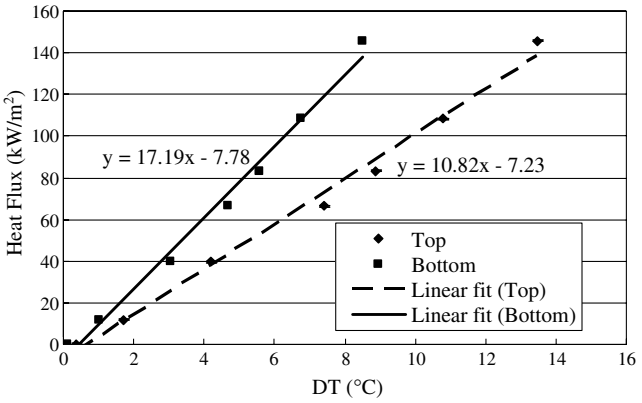

Fig. 5. Thermocouple pair calibration results for a typical cross-section.

ties in the temperature measurements. The relative error is higher for low heat flux due to the smaller temperature difference across the tube wall. An average error of ±10% was used for the data based on an error analysis of the system.

It should be noticed that this calibration only gives the relative distances between the inner and outer surface thermocouples; the absolute location of each thermocouple is still unknown. The absolute locations would be desirable when examining the temperature profiles as discussed in Section 5. However, the current calibration setup does not provide a reference location or temperature with which to anchor the relative distance along the wall thickness.

Further details of the heat flux measurement method are provided in [16].

4. Test conditions and procedures

The test conditions listed in Table 1 were determined by a scaling analysis of the PCCS system and extended to provide a larger database for physical understanding of the phenomena. The scaling was based on General Electric's 1190 MWe ESBWR design described by Challberg et al. [4]. This design has four PCCS units that condense steam from the containment drywell and transfer heat to outside water pools at a rate of 13.5 MW. The heat transfer rate corresponding to each tube is given as

$$Q_{\text{unit}} = N_{\text{tubes/unit}} Q_{\text{tube}} \tag{2}$$

The design described by Challberg et al. has 672 tubes in each unit. From the decay heat curve, the maximum heat transfer rate per tube corresponds to 20.0 kW which is the initial phase of the LOCA. From the decay heat curve, the heat transfer rate per tube after 72 h corresponds to 7.25 kW. These heat transfer rates define the maximum and minimum inlet steam mass flow rates into the condenser tube for LOCA conditions. The range of flow rates calculated from this heat transfer limit corresponds to 3.4–9.4 g/s.

Table 1
Test conditions

Parameter	Range
Primary side pressure (MPa)	0.1, 0.2, 0.4
Steam inlet flow rate (g/s)	6.0–46.0
Steam/air mixture inlet velocity (m/s)	8.2–38.0
Inlet Reynolds number of steam/air mixture	19,700–159,000
Noncondensable gas inlet mass fraction (%)	0–20
Secondary side coolant water flow rate (kg/s)	1.48
Secondary side coolant inlet temperature (°C)	45.0

From preliminary experiments, it was found that at 6.0 g/s steam flow rate, complete condensation occurs in the single tube facility even for the highest air mass fraction (20%). Therefore experiments of lower steam mass flow rates were not performed. For the upper limit of the steam flow rate, 9.4 g/s corresponds to only 20 kW of heater power, which is far below the capacity of the steam generator. Since the purpose of the current experiment is to provide a complete data base, the inlet steam velocities were extended to allow for annular and stratified flow and for condensate Reynolds numbers that cover the range of both laminar and turbulent flow. The upper limit of the inlet steam mass flow rate was 46.0 g/s, which corresponds to about 100 kW heater power.

The pressure range covers the design limit of a typical light water reactor containment. The range of inlet air mass fraction was chosen to cover the possible air mass fraction range under hypothetical accident scenarios.

The steam mass flow rate, air mass flow rate, inlet pressure, coolant inlet temperature and coolant flow rate were kept constant during each test. The steam mass flow rate was kept steady by having critical flow through a control valve on the steam line. The air mass flow rate was adjusted automatically by the air mass flow controllers. Manual control of a vent valve at the test section outlet determined the inlet pressure.

To obtain reliable data, the coolant flow must be reasonably uniform around the test section. The heat transfer rates would be greatly affected if the coolant were thermally stratified due to density difference. Prior to the experiments, a CFD calculation with simplified boundary conditions (constant condenser tube wall temperature) confirmed that the thermal stratification in the coolant flow was negligible (<1.0 °C).

The CFD simulation was performed using the commercial code FLUENT. Half of the coolant annulus (left or right half) was simulated as the computational domain. The first meter in the axial direction was calculated. The boundary condition on the condenser tube outer surface was set to be constant temperature at 90 °C, and the boundary condition on the coolant annulus outer diameter was set to be adiabatic. Coolant water viscosity and density were set to be a function of temperature and the coolant inlet temperature was the same as in the experiment (45.0 °C). Fig. 6 shows that the temperature difference from the top to the bottom is negligible.

The coolant flow rate in the experiments was controlled by adjusting the bypass flow rate of the coolant pump. The coolant inlet temperature was maintained at about 45 °C by re-circulating part of the heated coolant and mixing it

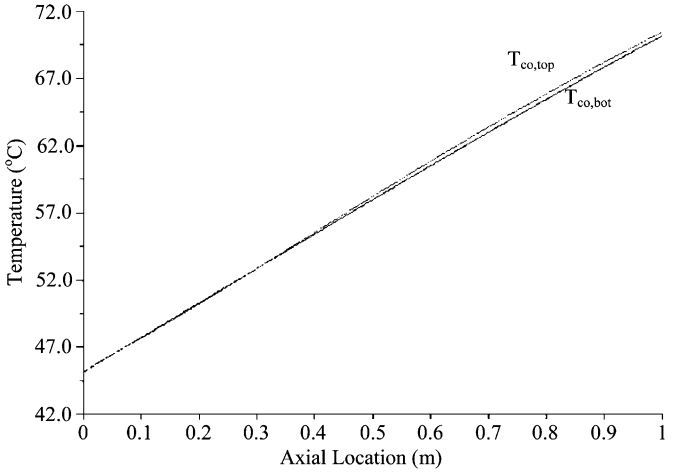

Fig. 6. CFD predictions of coolant temperature for inlet flow rate: 1.48 kg/s ($v = 0.60$ m/s).

with cooler city water. Data was recorded when the system had been at a steady state for at least 10 min. The approach to steady state was monitored by plotting control variables against time on the data acquisition PC.

5. Results and discussion

5.1. Axial temperature profiles

Fig. 7 shows the temperature profiles along the test section for one of the tests. The vertical lines in the figure show the axial locations of the local temperature measurement cross-sections. As expected, the temperature profiles reveal the highest temperatures along the centerline. The condenser tube inner surface temperatures are well below the centerline temperatures, with temperatures at the top of the tube being higher than those at the bottom of the tube. Finally, the temperature rise in the coolant running countercurrent to the primary side is evident.

By comparing the CFD results and the experimental results, the asymmetrical wall temperature and heat flux

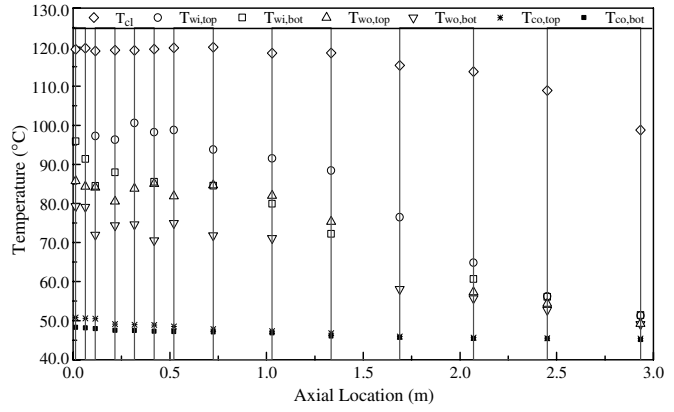

Fig. 7. Typical temperature profiles (inlet steam mass flow rate: 11.5 g/s, inlet air mass fraction: 5%, inlet pressure: 200 kPa), vertical lines represent the locations of temperature measurement cross-sections.

are concluded to have caused the asymmetrical coolant temperature. The density effect was minimal on coolant stratification.

The large difference in the "T_{wi}" and the "T_{wo}" profiles demonstrates the success of the new embedded thermocouple design. For most tests, the temperature drop across the condenser tube wall is as large as 15.0 °C. This temperature difference is large compared to the error associated with the thermocouples (±0.7 °C). Some other experimental programs employed a much thicker wall in order to obtain an accurate local heat flux measurement [17–19], but the heat flux is reduced due to the wall thickness.

The temperature dip in the condenser tube wall thermocouple readings in the first 0.3 m from the inlet is an unexpected result attributed to entrance effects. Complications near the inlet are common in condensation heat transfer facilities [6,20]. The uncertainties in the absolute positions of the thermocouple junctions have been raised as a possible contributor to this effect. However, experimental data showed that in the current experimental series, this effect does not appear consistently in the data. The temperature dip is significant only under high pressure and high mass flow rate test conditions, suggesting that the major cause is the entrance effect. One possible cause of this entrance effect is that near the inlet, there is strong condensation potential. Steam is sucked towards the interface and the diffusion of air towards the center of the tube is suppressed by the suction of steam towards the interface, resulting in a high interface air concentration. The interface temperature is low and, therefore the tube wall temperature is low.

Since the wall thermocouple junctions are embedded in the wall, the measured condenser tube inner and outer surface temperatures "T_{wi}" and "T_{wo}" are not the temperatures at the physical wall boundaries. These temperatures were corrected to the physical boundaries by a heat conduction calculation and labeled as "$T_{wall,in}$" and "$T_{wall,out}$" correspondingly.

5.2. Global effects of noncondensable gas

In many heat exchangers, the inlet flow of the condenser tube may contain a significant concentration of NC gas. The NC gas accumulates along the condensate film to form a boundary layer that inhibits steam from reaching the film surface. With a lower vapor partial pressure at the condensation surface, the heat transfer rate is decreased and the heat exchanger performance is degraded. For forced flow condensation, the effect of the noncondensable gas should be much less significant than in the case of a stagnant vapor because the mixing induced by the flow promotes steam contact with the heat transfer surface [21].

The effect of the NC gas can be examined by comparing the centerline temperature profiles (Figs. 8 and 9). The centerline temperature corresponds to the local steam saturation temperature. In these experiments, since the pressure drop along the heat transfer length is less than 1.0 kPa for most of the test conditions, the assumption that the

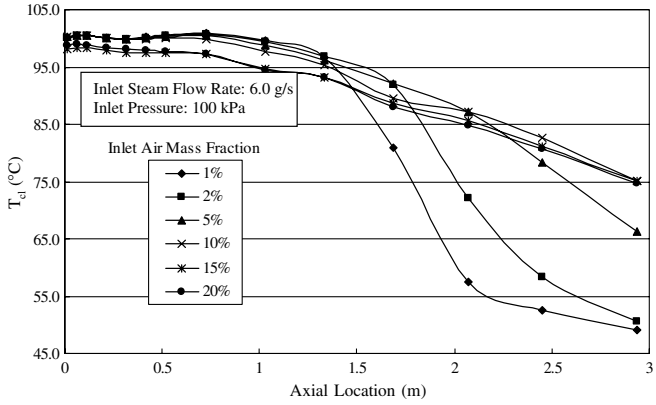

Fig. 8. Centerline temperature profiles for various inlet air mass fractions (inlet steam flow rate: 6.0 g/s, inlet pressure: 100 kPa).

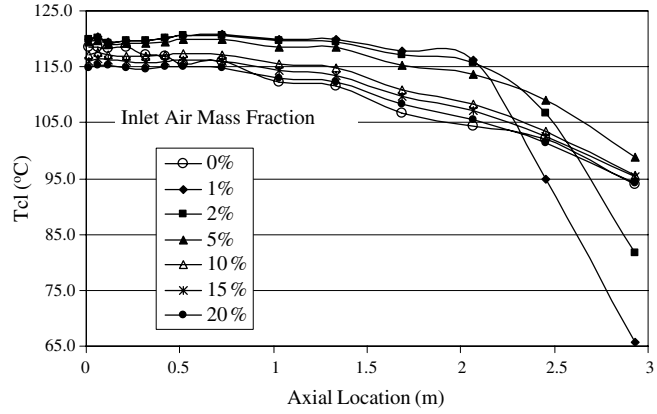

Fig. 9. Centerline temperature profiles for various inlet air mass fractions (inlet steam flow rate: 11.5 g/s, inlet pressure: 200 kPa).

centerline temperature reflects the local steam partial pressure is valid. At the inlet, the steam partial pressure is close to the total pressure. The difference with the total pressure at higher inlet air mass fractions is due to the air partial pressure. Therefore, the inlet temperature for the conditions with higher air mass fraction is relatively low due to the lower steam partial pressure.

With the mixture flowing through the condenser tube, the mixture temperature drops sharply after a major part of the steam has been condensed. From Fig. 8 it can be seen that the condensation length is shorter for lower air mass fraction cases because this source of thermal resistance is small. Also the condensate rate measurement by condensate collection confirmed that for the 10%, 15% and 20% inlet air mass fraction cases, steam had been vented out. For the 1%, 2% and 5% inlet air mass fraction cases, the condensate collection rate is close to the inlet steam mass flow rate. For the steam flow rate shown in Fig. 9, a pure steam test was performed. The inlet pressure could not be maintained due to complete condensation of the steam within the tube. The inlet pressure was about 70.0 kPa, which corresponds to a saturation temperature of 90 °C. Therefore, the inlet steam was superheated and the steam near the outlet was saturated. Other temperature profiles in Fig. 8 show the same trend, in which the 1% and 2% inlet air mass fraction cases exhibit complete condensation.

By comparing Figs. 8 and 9, the effect of inlet pressure can also be seen. From Fig. 8, it is expected that for 11.5 g/s inlet steam flow rate, 1% inlet mass fraction under 100 kPa inlet pressure, the condensation length would be much longer than that for 6.0 g/s inlet steam flow rate, perhaps greater than 3 m. From Fig. 9 it can be seen that for 11.5 g/s inlet steam mass flow rate and 1% inlet air mass fraction under 200 kPa inlet pressure, the condensation length is approximately 2.0 m. This means that for the same inlet steam mass flow rate and air mass fraction, the condensation length is shorter for high inlet pressure conditions. Fig. 10 shows the effect of pressure on local heat transfer coefficient profiles. The heat transfer coefficient is defined in a later section. From the comparison, the heat transfer coefficient profiles show a decreasing trend with increasing the inlet pressure. This trend is consistent with the classical Nusselt analysis for pure steam condensation. The same trend has also been observed in the experimental results of Oh and Revankar [22] for condensation in a vertical tube. Although consistent, the trend is rather insignificant, which means that there is very little effect from the pressure because the mixture shear and large temperature gradients dominate the heat transfer.

In the current experiment, air was used as the noncondensable gas and the effect of gas composition was not examined from the results. The degradation effect of lighter gases such as hydrogen or helium may be greater than for air since these lighter gases tends to accumulate at the top part of the tube due to the buoyancy effect. Future experiments will be performed on this effect.

5.3. Local flow regimes

In horizontal heat exchanger tubes, steam condenses along the inner surface of the tube and runs along the periphery to the bottom. The liquid film on the tube wall represents a resistance to the heat transfer. The major flow regimes are annular flow and stratified flow in the present

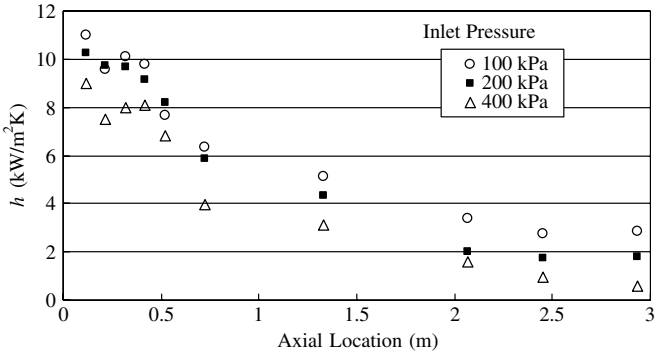

Fig. 10. Heat transfer coefficient profiles at the top of the tube for different inlet pressures (inlet steam mass flow rate: 11.5 g/s, inlet air mass fraction: 15%).

study. For annular flow, most of the current heat transfer models [10,11] treat the film thickness as being uniform. For stratified flow, the primary heat transfer modes at the tube bottom are conduction and forced convection; however, the thicker condensate layer at the bottom provides more heat transfer resistance, rendering the upper section of the tube a more effective heat transfer surface.

In a horizontal condenser tube, the local flow regimes strongly affect the heat and mass transfer processes. The most widely used flow regime map for horizontal two-phase flow was developed by Mandhane et al. [23] for adiabatic two-phase flow, in which the flow regimes were defined on a plot of the liquid superficial velocity vs. gas superficial velocity. For horizontal condensation flow, Jaster and Kosky [24] defined the major flow regimes as annular, transition and stratified flow based on their experimental observations of steam condensation in a 12.5 mm ID tube. Flow regime transition criteria were developed based on a force balance between the gravitational force and the wall shear stress. Soliman [25–27] investigated the condensation phenomena of refrigerants and classified the flow regimes into mist, annular and wavy flows. The modified Weber number was used to predict the mist-to-annular transition and the Froude number was used to predict the annular-to-wavy transition. Rifert [19] proposed a chart for horizontal condensing flow of steam and classified the flow regime as annular, asymmetric or gravitational flow based on the nature of local heat transfer coefficients distribution over the tube perimeter. These maps are of reference in determining the flow patterns in the current study. The Mandhane flow regime map is used because it is well established for adiabatic conditions and the Jaster and Kosky criteria is used because it is for steam condensation.

Since the local heat transfer characteristics are closely related to the flow regime, the flow regime at each local cross-section must be identified to analyze the heat transfer. To assess the local flow conditions, the local void fraction was estimated. The local coolant top and bottom temperatures were averaged to obtain the local average coolant temperature. Noting that the top and bottom temperatures are generally less than 5 °C apart, this is a reasonable simplification. The total heat transfer rate from the condenser tube inlet to the local cross-section could then be calculated by knowing the coolant temperature. The local condensate flow rate was calculated assuming the condensate at saturation state. The flow condition at a cross-section could then be approximately determined.

To identify the local flow regimes, both the Mandhane flow regime map [23] and the Jaster and Kosky flow regime identification criteria [24] were used and their results were compared. For most of the test conditions, the flow regime was either wavy flow or stratified flow regimes on the Mandhane flow regime map and transition or stratified flow according to the criteria by Jaster and Kosky:

$$F = \frac{\text{Axial shear force}}{\text{Gravitational body force}} = \frac{\tau_w}{\rho_l g \delta} \tag{3}$$

Here, the axial shear force is estimated by a two-phase multiplier method. In estimating the axial shear force and the film thickness, the film was assumed to be uniform around the periphery. By comparing the calculated F values and their observation of the flow regime inside the transparent condenser tube, Jaster and Kosky determined the flow regime transition criteria. For $F > 29$, the flow regime is annular flow, for $29 \geqslant F \geqslant 5$, the flow regime is transition flow and for $F < 5$, the flow regime is stratified flow. Fig. 11 shows the flow regime transition along the test section for all the inlet steam mass flow rates. The inlet air mass fraction was 5% for all the test conditions shown. When the inlet pressure and steam mass flow rate are kept constant, generally the local flow regime does not vary with inlet air mass fraction except for the pure steam tests. From Fig. 11, it can be seen that F decreases along the condenser tube. For the low mass flow cases, F comes to asymptotic value, signifying the finish of the condensation.

The flow regime analysis by the Mandhane flow regime map for the test conditions corresponding to Fig. 7 shows that the first three cross-sections ($z = 0.013, 0.064, 0.114$ m) were in the wavy flow regime. For the cross-sections downstream, the flow regime was stratified flow. The results using the Jaster and Kosky criteria show that only the first cross-section was in the transition flow regime and the rest of the cross-sections were in the stratified flow regime. This discrepancy could be caused by the definition of the flow regimes since both of authors defined the flow regimes by flow visualization.

5.4. Local heat transfer coefficients

From the temperature profiles, the local heat fluxes at the top and bottom of the tube were calculated with their corresponding calibration equations. The local heat transfer coefficients are defined as

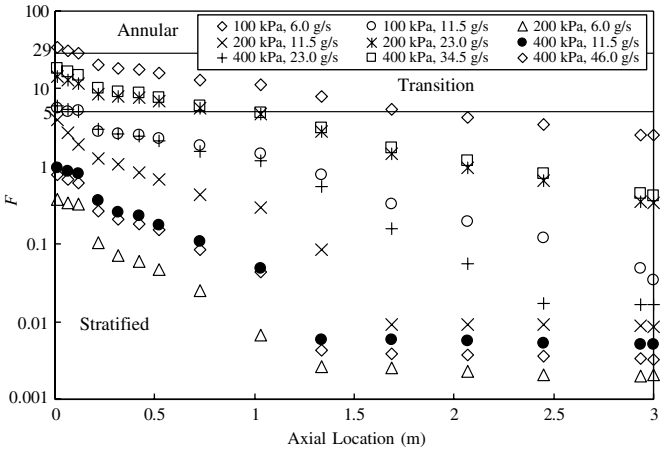

Fig. 11. Flow regime transition along the condensation length (inlet air mass fraction: 5%).

$$h_*(z) = \frac{q''_{\text{wall,in},*}(z)}{T_{\text{cl}}(z) - T_{\text{wall,in},*}(z)} \quad (4)$$

This heat transfer coefficient includes the condensation heat transfer coefficient and the condensate film heat transfer coefficient because no data on film characteristics are available to separate the two components. Fig. 12 shows the local heat transfer coefficient profile corresponding to the test conditions of Fig. 7.

The local heat transfer coefficient profile shows the highest value at the inlet of the condenser tube and a decrease along the condenser tube. This is due to the decrease of the steam/air mixture velocity, the increase of the condensate film thickness along the condenser tube and the increase of the local air concentration.

It can be clearly seen that near the inlet of the condenser tube, the heat transfer coefficients at the top of the tube are much higher than those at the bottom of the tube. This is mainly due to the asymmetrical film thickness profile. For certain low steam mass flow conditions, according to the flow regime transition criteria of El Hajal et al. [28] the flow regime is stratified from the inlet of the tube. Near the tube inlet, the condensate film is the major heat transfer resistance. Towards the outlet of the condenser tube, most of the steam has been condensed and the predominant heat transfer mechanism changes from condensation heat transfer to single-phase gas cooling by forced convection at the top of the tube. At the bottom of the tube, the heat transfer mechanism is forced convection through the condensate. Not much difference is shown between the top and bottom of the tube at the outlet. Heat transfer calculations without phase change were performed and the results showed that the temperature difference caused by single-phase heat transfer is far less than the uncertainties in the temperature differences measured by the thermocouple pairs (±0.7 °C). Thus the heat transfer coefficient in this region is out of the measurement capability of the thermocouple pairs which were developed for measuring phase-change heat transfer. Also, this low heat transfer region can be neglected since it is not of prime interest for the current research. Error bars were added to Fig. 12 to account for the error in the calibration and the uncertainties caused by the thermocouples.

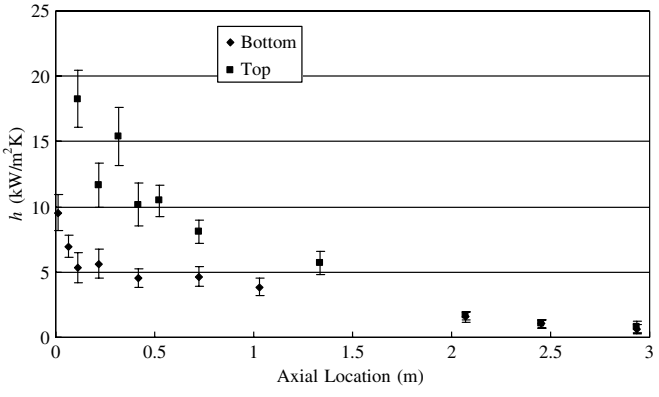

Fig. 12. Typical local heat transfer coefficient profiles.

5.5. Additional local heat transfer characteristics

From the typical local heat transfer coefficients, it can be seen that the top of the condenser tube is a much more efficient heat transfer surface. In this section, the local heat transfer characteristics are analyzed separately for the top and bottom for test conditions with the same inlet air mass fraction. Figs. 13 and 14 show the top and bottom heat transfer coefficients for test conditions of inlet air mass fraction 5%.

Fig. 13 shows the heat transfer coefficients for the top of the tube, where the x-axis is the local mixture Reynolds number. The approximate local air mass fraction is also shown in the figure. It is seen that the heat transfer coefficients at the inlet for different Reynolds number are approximately the same. Near the inlet, the major heat

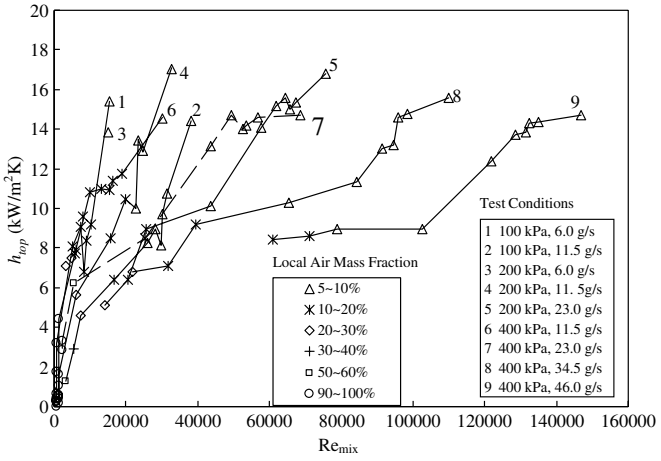

Fig. 13. Heat transfer coefficients at the top of the tube (inlet air mass fraction: 5%).

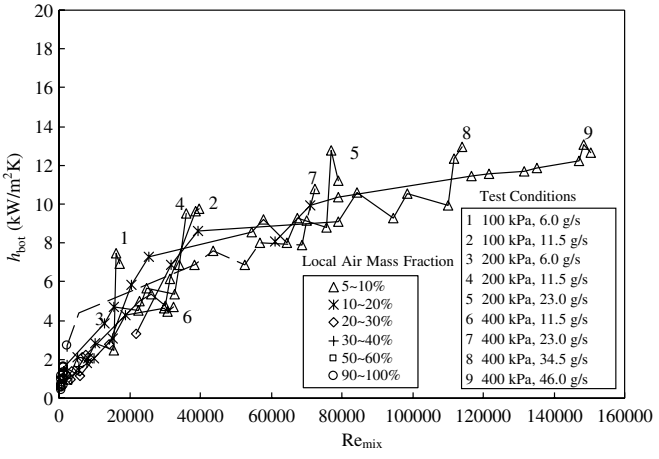

Fig. 14. Heat transfer coefficients at the bottom of the tube (inlet air mass fraction: 5%).

transfer mechanism is condensation of steam and the air concentration distribution in the cross-section is uniform. The dependency of the heat transfer coefficient on the mixture Reynolds number is very small.

As the mixture flows through the condenser tube, the mixture Reynolds number decreases and the local air mass fraction increases. From Fig. 13, for test conditions with a high inlet mass flow rate, the flow regime remains in the annular or transition flow regime and the heat transfer coefficient does not decrease rapidly. The turbulent mixing helps the steam to penetrate through the NC gas boundary layer and condense on the heat transfer surface. However, for the test conditions with a low inlet steam flow rate, the flow regime changes to stratified flow and the local air mass fraction increases rapidly. The heat transfer coefficient also drops rapidly and shows a large dependency on the mixture Reynolds number.

Towards the outlet of the condenser tube, for the test conditions with a low steam mass flow rate, most of the steam has been condensed and the heat transfer coefficients show a higher dependency on Reynolds number due to a change in the heat transfer mode from condensation to forced convection of the NC gas. The high inlet steam mass flow rate tests may have considerable steam in the mixture at the outlet and the local air mass fraction is still relatively low. The heat transfer coefficient is relatively constant in this region, with a slightly decreasing trend due to the build up of a NC gas boundary layer.

Fig. 14 shows the heat transfer coefficients at the bottom of the tube. In this figure, the heat transfer coefficient shows a larger dependency on the mixture Reynolds number in all tube regions compared to that at the top of the tube. For the test conditions with a high inlet steam mass flow rate, the heat transfer coefficients are less dependent on the mixture Reynolds number near the inlet. The flow regime near the inlet is annular or wavy flow and the heat transfer mode is still condensation of steam. For the test conditions with a low inlet steam mass flow rate, the heat transfer coefficient is highly dependent on the Reynolds number. The flow regime is stratified flow, the heat transfer mode at the bottom of the tube is forced convection of the condensate and the heat transfer is therefore highly dependent on the shear of the mixture.

From the above analysis, it can be seen that the factors affect the local heat transfer characteristics are the local air mass fraction, local air concentration distribution, local liquid film characteristics and the local turbulent mixing effect.

6. Conclusions

Condensation of steam in a horizontal heat exchanger with a noncondensable gas present has been experimentally studied. The condenser tube inner surface, outer surface and annular coolant channel temperature profiles were measured along the top and the bottom of the test section along with the condenser tube centerline. For the condenser tube inner surface temperature, an innovative thermocouple design was developed that allowed for nonintrusive measurements. From these and other data, local heat fluxes were obtained for a variety of pressures, steam inlet velocities and noncondensable gas mass fractions.

The local heat fluxes are essential for development of analytical models of horizontal condensation heat exchangers but have not been seen reported elsewhere. In particular, it is important to distinguish the difference in performance between the top and bottom of the condenser tube to evaluate the overall performance. The experimental results also identified that the major flow regimes in the horizontal condenser tubes are generally wavy and stratified flow, with annular flow occurring only for a steam/air mixture velocity greater than about 35 m/s.

The global effect of NC gas on the heat transfer rate was investigated by comparing the centerline temperature profiles and the overall heat transfer rates. For the low inlet air mass fraction conditions studied in this paper, the effect is not as significant as expected.

The effect of the local air mass fraction, local air concentration distribution, local liquid film characteristics and the local turbulent mixing on the local heat transfer coefficient were qualitatively analyzed. The top and bottom show different dependencies on these factors due to the local flow conditions.

As future work, data at different angles and for different noncondensable gases will be obtained, quantitative analysis of the data will be performed and mechanistic models based on further data evaluation will be developed.

Acknowledgements

The authors gratefully acknowledge financial support of this project by the US Department of Energy Nuclear Engineering Education Research (NEER) Project, Award No. DE-FE07-02ID14341. The assistance of Mr. Yong Jae Song in conducting the experiments is also appreciated.

References

[1] S. Kakac, H. Liu, Heat exchangers selection rating and thermal design, in: Condensers and Evaporators, CRC Press, New York, 1998.
[2] H. Nakamura, Single U-tube testing and RELAP5 code analysis of PCCS with horizontal heat exchanger, in: NTHAS2: Second Japan–Korea Symposium on Nuclear Thermal Hydraulics and Safety, Fukuoka, Japan, 2000, pp. 336–343.
[3] B.S. Shiralkar, M. Alamgir, J.G.M. Andersen, Thermal hydraulic aspects of the SBWR design, Nucl. Eng. Des. 144 (1993) 213–222.
[4] R.C. Challberg, Y.K. Cheung, S.S. Khorana, H.A. Upton, ESBWR evolution of passive features, in: 6th International Conference on Nuclear Engineering (ICONE-6), San Diego, USA, 1998, pp. 1–10.
[5] W.M. Rohsenow, Section 12, part a, film condensation, in: Handbook of Heat Transfer, McGraw-Hill, New York, 1973.
[6] K. Vierow, Behavior of steam–air systems condensing in concurrent vertical downflow, M.S. thesis, University of California, Berkeley, California, 1990.

[7] F. Blangetti, R. Krebs, E.U. Schlunder, Condensation in vertical tubes – experimental results and modeling, Chem. Eng. Fund. 1 (2) (1982) 20–42.
[8] P.F. Peterson, C.L. Tien, Mixed double diffusive convection in thermosyphons, J. Heat Transfer 112 (1990) 78–83.
[9] J.C. Chato, Laminar condensation inside horizontal and inclined tubes, Am. Soc. Heating Refrig. Air Cond. Engns. (ASHRAE) J. 4 (1962) 52–60.
[10] M.M. Shah, A general correlation for heat transfer during film condensation inside pipes, Int. J. Heat Mass Transfer 22 (1979) 547–556.
[11] M.K. Dobson, J.C. Chato, Condensation in smooth horizontal tubes, J. Heat Transfer 120 (1998) 193–213.
[12] T. Ueno, N. Nakamori, T. Matsuoka, K. Okabe, T. Sugisaki, J. Kodama, Study on core cooling of hybrid safety system for next-generation PWR during LOCA, in: The 3rd JSME/ASME Joint International Conference on Nuclear Engineering, Kyoto, Japan, 1995, pp. 963–969.
[13] H.F. Rosson, J.A. Meyers, Point values of condensing film coefficients inside a horizontal tube, Chem. Eng. Prog. Symp. Ser. 61 (59) (1965) 190–199.
[14] S.Z. Kuhn, Investigation of heat transfer from condensing steam-gas mixtures and turbulent films flowing downward inside a vertical tube, Ph.D. thesis, University of California, Berkeley, California, 1995.
[15] P.F. Peterson, V.E. Schrock, T. Kageyama, Diffusion layer theory for turbulent vapor condensation with noncondensable gases, J. Heat Transfer 115 (1993) 998–1003.
[16] T. Wu, K. Vierow, A local heat flux measurement technique for inclined heat exchanger tubes, Exp. Heat Transfer 19 (1) (2006) 1–14.
[17] H. Araki, Y. Kataoka, M. Murase, Measurement of condensation heat transfer coefficient inside a vertical tube in the presence of noncondensible gas, J. Nucl. Sci. Technol. 32 (6) (1995) 517–526.
[18] T. Chataing, P. Clement, J. Excoffon, General correlation for steam condensation in case of wavy laminar flow along vertical tubes, in: Ninth International Topical Meeting on Nuclear Reactor Thermal Hydraulics (NURETH-9), San Francisco, USA, October 3–8, 1999.
[19] V.G. Rifert, Heat transfer and flow modes of phases in laminar film vapour condensation inside a horizontal tube, Int. J. Heat Mass Transfer 31 (3) (1988) 517–523.
[20] P.F. Peterson, V.E. Schrock, S.Z. Kuhn, Recent experiments for laminar and turbulent film heat transfer in vertical tubes, Nucl. Eng. Des. 175 (1997) 157–166.
[21] E.M. Sparrow, W.J. Minkowycz, M. Saddy, Forced convection condensation in the presence of noncondensables and interfacial resistance, Int. J. Heat Mass Transfer 10 (1967) 1829–1845.
[22] S. Oh, S.T. Revankar, Analysis of the complete condensation in a vertical tube passive condenser, Int. Commun. Heat Mass Transfer 32 (6) (2005) 716–727.
[23] J.M. Mandhane, G.A. Gregory, K. Aziz, A flow pattern map for gas–liquid flow in horizontal pipes, Int. J. Multiphase Flow 1 (1974) 537–553.
[24] H. Jaster, P.G. Kosky, Condensation heat transfer in a mixed flow regime, Int. J. Heat Mass Transfer 19 (1976) 95–99.
[25] H.M. Soliman, On the annular-to-wavy flow pattern transition during condensation inside horizontal tubes, Can. J. Chem. Eng. 60 (1982) 475–481.
[26] H.M. Soliman, Correlation of mist-to-annular transition during condensation, Can. J. Chem. Eng. 61 (1983) 178–182.
[27] H.M. Soliman, The mist-annular transition during condensation and its influence on the heat transfer mechanism, Int. J. Multiphase Flow 12 (2) (1986) 277–288.
[28] J. El Hajal, J.R. Thome, A. Cavallini, Condensation in horizontal tubes. Part 1. Two-phase flow pattern map, Int. J. Heat Mass Transfer 46 (18) (2003) 3349–3363.